Received: 1/12/2025/Accepted: 19/1/2026

Non-Isolated Bidirectional Half-Bridge Architecture for Hybrid Energy Storage System in Photovoltaic Microgrids: Evaluation in PSIM

Arquitectura *half-bridge* bidireccional no aislado para sistema de almacenamiento híbrido en microrred fotovoltaica: evaluación en PSIM

Nancy Reynosa Casas nancyreynosa6@gmail.com (1)
https://orcid.org/0009-0002-6047-0592

Yusbel Llorrente Cutiño rentecutinoyusbel@gmail.com (2)
https://orcid.org/0009-0004-6625-1096

Christian E. Borges Alvarez christianborges696@gmail.com (1)
https://orcid.org/0009-0000-5215-9812

Yilena Paumier Leyva ypaumierl@ismm.edu.cu (1)
https://orcid.org/0009-0002-5858-3483

Osmany R. Pérez Aballe* opaballe@ismm.edu.cu (1)
https://orcid.org/0000-0001-6425-071X

(1) University of Moa, Moa, Cuba (2) Electric Company, Sagua de Tánamo, Cuba
*Corresponding author

Abstract: This paper describes how the power electronics software PSIM was used to design and simulate a bidirectional full-bridge DC–DC converter to integrate a hybrid storage system into a photovoltaic microgrid. The objective is to manage power flow between sources and storage devices in order to smooth transients, reduce current stress on the battery, and maintain appropriate voltage levels on the DC bus. Due to the limitations in the evaluation version of the circuit simulation program, equivalent elements were employed to reproduce the quasi-stationary behavior of the photovoltaic array, the battery bank, and the super capacitor module. Seven representative operating scenarios were analyzed (charging/discharging in both directions, supercapacitor support, and power transfer from/to generation), evaluating key voltages and currents. The results demonstrate effective bidirectionality and high-frequency power decoupling capability provided by the supercapacitor, with positive implications for battery lifetime. In addition, a prototype-level cost estimation is included, and limitations and future work focused on dynamic control and experimental validation are discussed.

How to cite: Reynosa-Casas, N., Llorrente-Cutiño, Y., Borges-Alvarez, C. E., Paumier-Leyva, Y., & Pérez-Aballe, O. R. (2026). Non-Isolated Bidirectional Half-Bridge Architecture for Hybrid Energy Storage System in Photovoltaic Microgrids: Evaluation in PSIM. *Ciencia & Futuro, 16.* https://revista.ismm.edu.cu/index.php/revistacyf/article/view/2893

Key words: electrical converters, electric power, electronic equipment

Resumen: Se presenta el diseño y la simulación en el *software* para la electrónica de potencia PSIM de un convertidor DC–DC bidireccional tipo puente completo para integrar un sistema híbrido de almacenamiento de energía en una microrred fotovoltaica. El objetivo es gestionar el flujo de potencia entre las fuentes y los almacenadores para suavizar transitorios, reducir el estrés de corriente en la batería y mantener niveles de tensión adecuados en el bus DC. Dadas las limitaciones de la versión de evaluación del programa de simulación de circuitos, se emplean elementos equivalentes para reproducir el comportamiento cuasi-estacionario del arreglo fotovoltaico, del banco de baterías y del módulo de supercondensadores. Se analizan siete escenarios de operación representativos (carga/descarga en ambas direcciones, soporte del supercondensador, y transferencia desde/hacia la generación), evaluando tensiones y corrientes clave. Los resultados muestran bidireccionalidad efectiva y capacidad de desacoplo de potencia de alta frecuencia por parte del supercondensador, con implicaciones positivas sobre la vida útil de la batería. Se incluye, además, una estimación de costes a nivel de prototipo y se discuten limitaciones y trabajo futuro orientado a control dinámico y validación experimental.

Palabras clave: convertidores eléctricos, equipamiento electrónico, energía eléctrica

1. Introduction

The increasing penetration of variable renewable sources into microgrids requires storage solutions that enable coupling generation and demand while mitigating intermittency and power peaks (Faisal *et al*., 2018). In this context, Hybrid Energy Storage Systems (HESS) combine high specific energy devices (LFP batteries) with high specific power devices (supercapacitors), so that each technology operates near its optimal zone (Ramos *et al.*, 2022; Wang *et al.,* 2022). Supercapacitors attenuate transients and current pulses, while batteries supply average energy, reducing its high-amplitude charge/discharge cycles and, consequently, its degradation (Tremblay & Dessaint, 2009; Zhang *et al.,* 2017; Zubieta & Bonert, 2000; Eaton, 2023; Winston Battery, 2024; Pérez-Aballe *et al*., 2025).

To exploit these advantages, it is essential to count on a bidirectional DC-DC converter capable of directing the energy flow from the photovoltaic source to the DC bus and storage devices, as well as between the storage devices, in both directions (charging/discharging) (Mohan *et al.,* 2003; Ardi *et al.,* 2014; Erickson & Maksimović, 2020; Sutikno *et al*., 2023). This paper addresses the design and simulation of a bidirectional half-bridge converter to interconnect the DC bus with the battery bank and the supercapacitor module.

For this study, the circuit simulation program (PSIM) is particularly relevant as it is oriented towards power electronics, featuring switched and averaged models, control blocks (Pulse Width Modulation PWM, comparators, PI), and dependent sources that reproduce the behavior of a bidirectional half-bridge and the battery–supercapacitor energy exchange in a rapid and stable way. Additionally, it eases the establishment of initial conditions, performance of parametric sweeps, and measurement of key variables (iL, Vbus, VSC), which aligns with the quasi-stationary scenario-based approach adopted. Additionally, its simulation speed in multi-purpose environments makes it ideal for preliminary design and concept validation in DC microgrids with HESS (Powersim, 2022).

Within this framework, the study focuses on representative scenarios, taking into account the restrictions of the evaluation version, in order to: (I) verify bidirectionality and power flow continuity, (II) observe the supercapacitor´s role into transient damping, and (III) establish sizing bases for inductance, capacitance, and semiconductors, relying on classical design criteria and gate driver application notes (Infineon Technologies, 2017; Erickson & Maksimović, 2020; Powersim, 2022).

Contributions: (1) Synthesis of requirements and half-bridge topology suitable for HESS in PV microgrids (Lin *et al*., 2013; Ardi *et al.,* 2014; Liu *et al.,* 2016; Tuluhong *et al.,* 2025); (2) simulation model in PSIM with practical equivalents allowing exploration of seven operating scenarios (Powersim, 2022); (3) comparative analysis of voltages and currents evidencing the supercapacitor's rapid discharge/recharge and consequent battery stress reduction (Zubieta & Bonert, 2000); (4) prototype cost estimation and discussion of limitations and future study, based on converter design criteria and gate drivers practical handling.

1.1. HESS Topologies

As shown in Figure 1, battery–supercapacitor HESS are usually classified as passive, semi-active, and active according to the degree of electronic conditioning and available control (Sutikno *et al.,* 2023). This taxonomy is linked to power distribution, battery stress, and overall system efficiency (Mohan *et al.,* 2003).

Passive ESS (Figure 1a): Batteries and supercapacitors (SC) directly connected to the DC bus, without dedicated converters. It is the simplest and most economical option, but power distribution depends on internal impedances and state of load, which can cause current peaks and mismatch losses, accelerating battery aging and

reducing efficiency (Faisal *et al*., 2018). The SC attenuates transients due to its low ESR, though without fine active control (Tshiani & Umenne, 2022).

Semi-active: one of the storage devices is connected via a bidirectional converter, allowing some control over the flow and voltages/currents (Sutikno *et al*., 2023).

- Semi-active SC (Figure 1b): the supercapacitor is coupled through the converter, and the battery is directly connected to the bus. It improves the SC use for peaks and ripple; however, the battery remains exposed to unregulated medium-frequency current variations (Bonert, 2000).

- Semi-active battery (Figure 1c): the battery is the one connected via the converter, while the SC is directly connected. This variant protects the battery against peaks (by limiting its current and diverting transients to the SC), which positively impacts its lifespan (Tremblay & Dessaint, 2009; Ramos *et al.,* 2022).

Active: both elements are connected via bidirectional converters ("active parallel" architecture), enabling independent power and State of Charge (SoC) control in each branch, as well as an optimal energy/power distribution (Tuluhong *et al.,* 2025).

- Parallel topology (Figure 1d): battery and SC with their own converters; the SC handles fast transients, the battery covers sustained demands, and the control coordinates the distribution (Lin *et al*., 2013; Lai *et al.,* 2015; Liu *et al*., 2016; Erickson & Maksimović, 2020).

- Cascaded topology (Figure 1e): the SC is placed between the battery and bus to act as a dynamic "filter" that isolates the battery from peaks at the expense of additional conversion stages and slight efficiency losses (Wang *et al.,* 2022).

Each approach involves a compromise between cost, complexity, and performance. Passive configurations are suitable for areas, such as remote microgrids, where simplicity and robustness are prioritized. Active ones are suitable for precise control, and semi-active ones offer a middle ground (Figure 1).

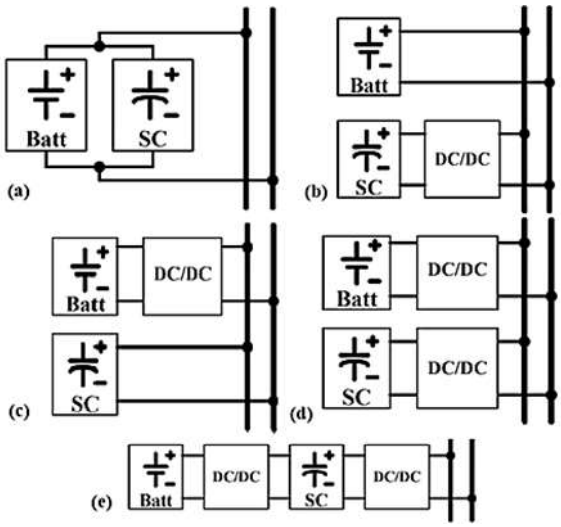

Figure 1. HESS management configurations in microgrids (Jing *et al*., 2017). a) Passive. b) Semi-active SC. c) Semi-active Battery. d) Active parallel. e) Active series.

1.1.1. Key Components and Characteristics

The HESS sizing relies on three interrelated metrics: energy density (Wh/kg or Wh/L), power density (W/kg), and durability/cycles (Pérez-Aballe *et al.,* 2025). Ragone's plot shown in Figure 2 summarizes the trade-off: batteries occupy the energy side, supercapacitors the power aspect, and other technologies (inertia flywheels, hydro-pneumatic systems) are distributed according to their physical characteristics and cost.

-Batteries (LFP): high energy density (≈100–250 Wh/kg), round-trip efficiency >90 %, and good cost per kWh. Limitations under sustained power (high C-rates → heating and aging). The Energy Management System (EMS) must limit current, manage temperature, and plan DoD/cycles; incorporating degradation models is advisable to minimize LCOS.

-Supercapacitors: very high-power density (kW/kg), μs–ms response, and a million-cycle lifespan; ideal as a buffer for peaks/transients. Trade-off: low specific energy and higher cost per kWh → complementary use, not as primary storage.

-Flywheels and hydro-pneumatic systems: high power and durability, but involve mechanical/cost demands that restrict their application to stationary or larger-scale installations.

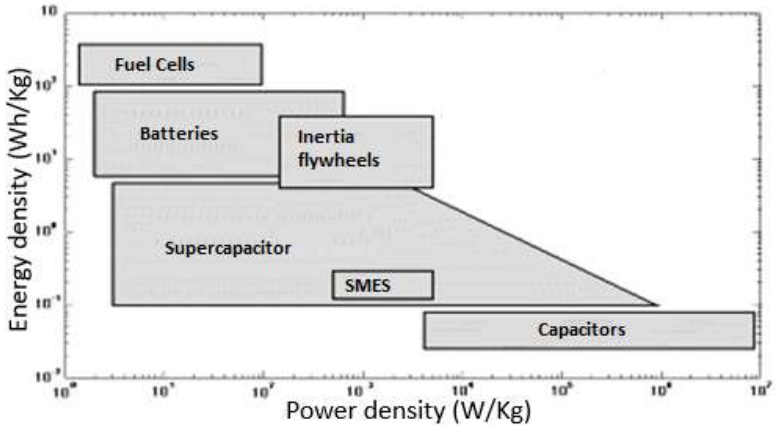

Figure 2. Ragone´s plot for energy storage analysis (Pérez-Aballe *et al.,* 2025).

1.2. LFP Batteries and Supercapacitors: models and characteristics

In HESS, batteries and supercapacitors are combined because they offer complementary features: batteries provide energy (autonomy) but have a higher internal resistance and suffer from sustained peaks; SCs provide power (μs–ms pulses) and lighten battery stress, extending its lifespan. The joint performance also depends on the topology (passive, semi-active, active), which defines how both storage devices are connected and controlled (Pérez-Aballe *et al.,* 2025).

An extended Thevenin equivalent is used for LFP battery modeling, as shown in Figure 3:

- Controlled voltage source (VOC) in series with Rs and two RC branches (R_1–C_1, R_2–C_2) capturing the diffusion dynamics (solid/electrolyte).

- States: SoC, V_1, V_2. Input: current I. Output: terminal voltage V_T.

- Dependencies: VOC and parameters (Rs, R_1, C_1, R_2, C_2) vary with SoC, temperature, and current direction.

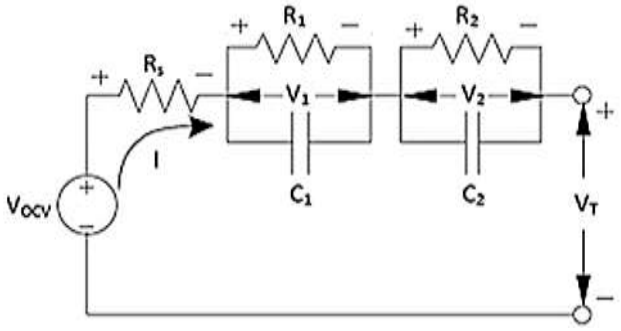

Figure 3. Lithium batteries' electrical model using a controlled voltage source.

The double layer supercapacitor (EDLC) modeling is structured by a double layer with very low internal resistance (ESR) and possible pseudo-capacitance, so the Q–V relationship can be non-linear. In practice, it is modeled with several RC branches to cover different time constants.

- Energy: $E = \frac{1}{2}CV^2$

- Series/parallel: series connection increases allowable V but decreases equivalent C; parallel connection increases C and allowable current.

- Modeling challenges: choosing the number of RC branches, considering V-dependent C or not, and estimating time constants and parameters (identification).

2. Materials and Methods

2.1 Bidirectional Half-Bridge DC-DC Converters Modeling

Bidirectionality is achieved with transistors operating as controlled switches (MOSFET/IGBT) and switching patterns enabling buck mode and boost mode between the DC bus and the storage device. The bidirectional half-bridge stands out for its simplicity and efficiency in HESS.

- Buck (charging): $V_L = V_{bus}D\text{-}V_{Alm}$; current increases/decreases according to duty, duty D and voltage differences.

- Boost (discharging): the inductor is energized from the storage device and transfers energy to the bus; Δi_LaVDT/L.

Figure 4 shows the electrical model of the non-isolated half-bridge converter.

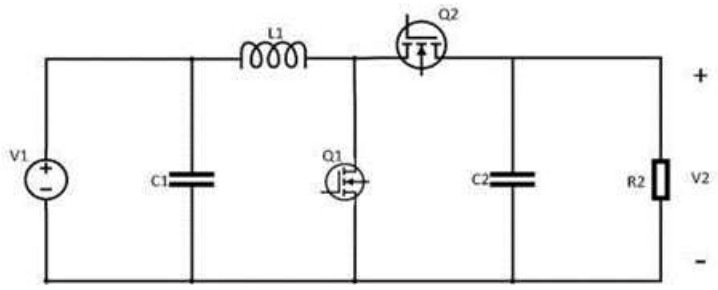

Figure 4. Electrical diagram of the half-bridge converter.

2.1.1. Buck Mode

According to Figure 5a), switch Q1 is conducting and Q2 remains off.

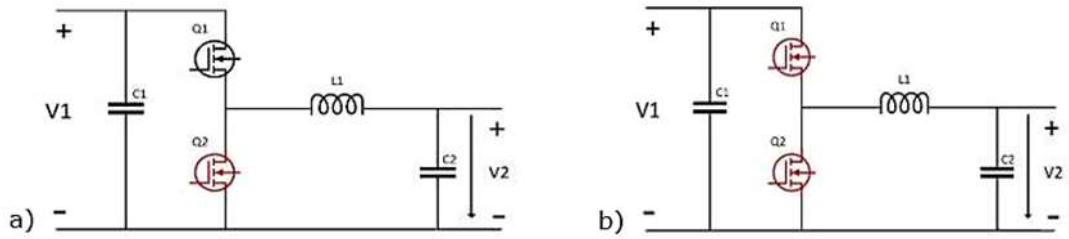

Figure 5. Half-Bridge Converter. Buck Mode. a) Q1-On, Q2-Off. b) Q1-Off, Q2-Off.

Under these conditions, the equivalent circuit is governed by equation (1). The temporal evolution of the inductor current is obtained from it, developing the procedure shown in equations (2) to (4), until reaching the final expression of equation (5) which results after solving and integrating the previous relations.

$$-V_1 + V_L = 0 \quad [1]$$

$$-L\frac{di_L}{dt} + V_L = 0 \quad [2]$$

$$V_L = L\frac{di_L}{dt} \quad [3]$$

$$\frac{V_L}{L} = \frac{di_L}{dt} \quad [4]$$

$$\frac{\Delta i_L}{\Delta t} = \frac{V_1 \mathrm{Dt}}{L} \quad [5]$$

According to Figure 5(b), Q1 and Q2 are both off. Under these conditions, the equivalent circuit is described by equation (6), from which the temporal evolution of the inductor's current is determined, following the corresponding analytical development.

$$-V_1 + V_L + V_2 = 0 \quad [6]$$

Considering the previous equation, the corresponding solving is performed until reaching equation (7), which is the desired response.

$$\frac{\Delta i_L}{\Delta t} = \frac{(V_1 - V_2)(1 - D)T}{L} \quad [7]$$

2.1.2. Boost Mode

Figure 6 shows the model of the half-bridge converter operating in boost mode. In Figure 6(a), switch Q1 conducts and Q2 remains cut-off; the equivalent circuit is established from the common equation (5). With this relation, an analysis is developed through the proposed equations, obtaining the inductor's current temporal evolution throughout the simulation interval.

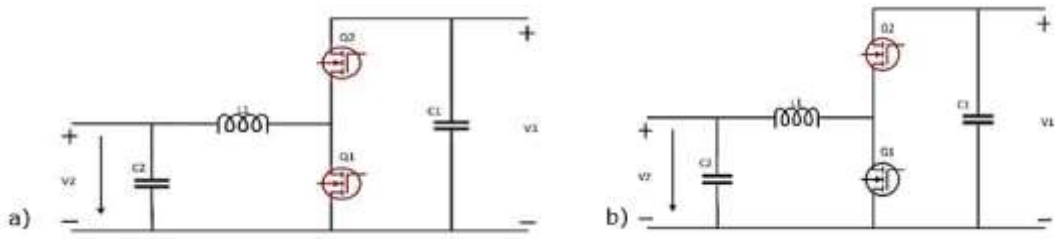

Figure 6. Half-Bridge Converter. Boost Mode. a) Q1-On, Q2-Off. b) Q1-Off, Q2-Off.

Upon performing this mathematical procedure, the response obtained is shown in equation (8), where it is observed that the inductor's current variation over time depends on the input voltage, the duty cycle, and the inductance value.

$$\frac{\Delta i_L}{\Delta t} = \frac{V_1 DT}{L} \quad [8]$$

Advantages: fine power control, active parallel integration, and compatibility with droop/integral-droop. Here, PSIM is used to represent the half-bridge and explore scenarios.

2.2. Bidirectional Converter Design, Scheme, and Operating Modes (Buck/Boost)

Figure 7 shows the bidirectional Half-bridge converter with two active switches and intrinsic diodes; complementary PWM with dead-time (dead-time between semiconductors activation.

Inductor L between the midpoint node and the storage device (V_{alm}); DC bus on the upper side.

Buck (charging):

$$V_{Sto} \approx DV_{bus};\ \Delta i_L = [(V_{bus} - V_{Stor})D]/(Lfs) \quad [9]$$

Boost (discharging):

$$V_{Sto} \approx DV_{bus}/(1-D);\ \ \Delta i_L = (V_{Sto}D)/(Lfs) \qquad [10]$$

Strategy in PSIM: duty D for objective to V/I; i_L measurement to limit ripple and avoid saturation; initial conditions (IC) in battery/SC.

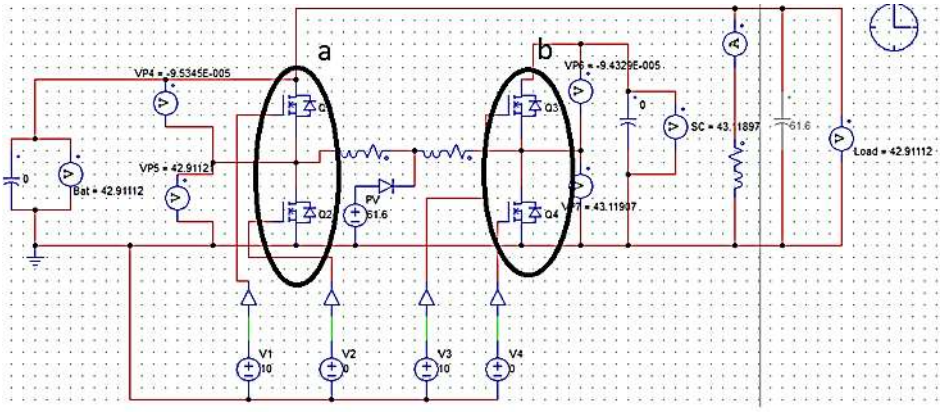

Figure 7. Electrical scheme of DC-DC converter model simulation in PSIM.

2.2.1. Parameters and Sizing (L, C, Semiconductors)

Ripple objective: For P ≈ 3 kW and V_{bus} ≈ 60 V → I_{avg} ≈ 50 A; set $\Delta i_L \leq 10$ A (20%).

Inductance L (worst cases):

- Buck (battery, V_{Sto}= 33 V, D ≈ 0.55): L ≈ 74 μH

- Boost (battery, V_{Sto}= 33 V, D ≈ 0.55): L ≈ 74 μH

- Buck (SC, V_{Sto} = 48.6 V, D ≈ 0.81): L ≈ 46 μH

Selection: L=80 μH, gapped core (airgap), I_{sat}≥70 A; I_{pk} ≈ 55 A

Capacitors: bus ΔV≤0.5% → C_{bus}≈1.0 mF (film + electrolytic + ceramics). Storage side: 100–220 μF + ceramics.

Semiconductors: 100 V MOSFET low-RDS(on); losses $P_{cond} \approx I_{rms}^2 \cdot$RDS (on); Psw≈0.5·V·I·(tr+tf)·fs.

Driver: 100 V bootstrap; Rg for dI/dt; *dead-time* 100–200 ns; snubbers if overshooting occur.

Measurement and protection: sensor in L, NTC/PTC, OVP/UVP, limiting per cycle.

PSIM Notes: time step 1–5 μs (fs = 20 kHz); record i_L, V_{alm}, V_{bus}, and duty.

2.3. Simulation Methodology, Environment, and Assumptions (PSIM)

Tool: PSIM (demo). Ideal models with realistic parameters and minimal parasitic signals.

Topology: half-bridge between DC bus and active storage device; AC inverter represented as an equivalent load on the bus (R–C). fs = 20 kHz; time step 1–5 μs (nominal 2 μs); complementary PWM with dead-time (100–200 ns).

IC: Vbus,0 = 60 V; V_{bat}, 0∈ [36,38] V; VSC,0 = 48.6 V. Signals: i_L, V_{bus}, V_{bat}, V_{SC}, *duty D*, P_{bus}, P_{bat}, $P_{SC.}$

Criteria: $\Delta V_{bus}/V_{bus} \leq 0.5$ %; $\Delta i_L \leq 20$ %·I_{avg}; $I_{pk} < I_{sat}$; sufficient SC energy.

Best practices: to record only key signals, use ICs per scenario, and verify steady states in advance to steps.

2.3.1. Analyzed Operating Scenarios

Seven quasi-stationary scenarios (100–300 ms; measuring after 3–5 τL):

- E1 Battery charging (buck)
- E2 Battery discharging (boost)
- E3 SC charging (buck)
- E4 SC discharging (boost)
- E5 PV→Bus smoothing with SC support
- E6 Peak with mixed support (SC+bat)
- E7 SC recharging from battery (buck)

Variables: V_{bus}, V_{bat}, V_{SC}, I_L, D, P_{bus}, P_{bat}, P_{SC}; ripple metrics, energies (∫p·dt), and I_{bat} peaks.

3. Results and Analysis

3.1. Battery, Supercapacitor, and Load Voltages per Scenario

In all cases, the analyzed elements are: (I) relative bus ripple, (II) inductor ripple, (III) continuity of I_L, and (IV) instantaneous powers. E1: $V_{bus} \approx 60$ V, continuous I_L, D ≈ 0.55–0.67. E2: D ≈ 0.45, P_{bat} positive towards bus. E3: V_{SC}→48.6 V; low ΔV_{bus}

due to C_{bus}. E4: SC handles pulse; V_{bus} within 0.5%; V_{SC} decreases according to energy delivered. E5: SC provides fast component; Δi_{bat} decreases. E6: SC handles the front and the battery takes over; $P_{SC} \rightarrow 0$ at the end. E7: SC recharging from battery with current limit and minimal impact on the bus.

Table 1 shows each stage characteristics and the most significant results for each one. Figure 8 illustrates the trends of the battery, load, and supercapacitor voltages behavior.

Table 1. Summary of results per operating scenario

Scenario	Dominant Flow	ΔVbus	ΔiL	Key Result
E1	Bus → Battery (buck)	≤0.5%	≤20%	Stable charging, SOC↑
E2	Battery → Bus (boost)	≤0.5%	≤20%	Load support, regulated bus
E3	Bus → SC (buck)	≤0.5%	≤20%	VSC to nominal, stored energy
E4	SC → Bus (boost)	≤0.5%	≤20%	Pulse handled by SC, VSC↓
E5	PV/Bus with SC	≤0.5%	≤20%	Ibat smoothing
E6	SC + Battery	≤0.5%	≤20%	Coordinated delivery, smooth transfer
E7	Batería → SC (buck)	≤0.5%	≤20%	SC recharge with minimal impact

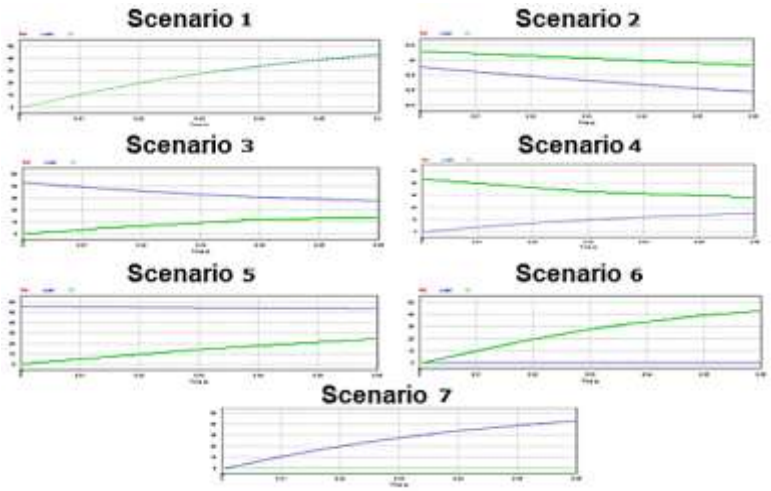

Figure 8. Battery, load, and supercapacitor voltages behavior per scenario.

3.2. Discussion and Limitations

The results confirm that the Supercapacitor rapidly absorbs/delivers the current component, while the battery sustains the average energy: bus ripples ≤0.5%, iL continuity, and I_{bat} peaks reduction. Selecting L = 80 μH and $C_{bus} \approx 1$ mF is adequate for 3 kW@60 V and fs = 20 kHz.

Limitations: quasi-stationary study without full control; simplified thermal and switching losses; demo PSIM restrictions.

Forthcoming work: current/power control with limits and anti-windup; SoC-dependent distribution; thermal models; HIL validation.

3.3. Technical-economic assessment of the prototype

Scope: Cost estimate for a functional bidirectional converter prototype (3 kW @ 60 V, fs = 20 kHz). Indicative market values in euros (± 20–30%).

Table 2. Bill of materials for the converter construction

Ítem	Specification	Qty.	Cost (€)	Subtotal (€)
100 V low-RDS (on) MOSFET	Parallel 2× per branch (4 pcs)	4	6–8	24–32
High/low-side driver	Bootstrap 100 V, UVLO	1	10–20	10–20
Inductor L	80 µH, Isat ≥70 A (gapped core + Litz)	1	50–90	50–90
Bus Capacitors	Film + electrolytic + ceramics (≈1 mF @ 63–80 V)	1 set	20–40	20–40
Current Sensor	100 A Hall or Kelvin shunt	1	15–35	15–35
Power PCB	FR-4, 4 layers, 2 oz Cu (≈100×100 mm)	1	40–80	40–80
Dissipation	Heatsink+ fan	1	25–45	25–45
Snubbers/RC/NTC/	Passives and power connectors	1 set	20–35	20–35
Case	Metal/plastic case	1	20–40	20–40
Converter's total cost: ~250–400 € (≈83–133 €/kW)				

4. Conclusions

The study confirms the suitability of a bidirectional half-bridge converter for integrating a battery–supercapacitor HESS into a PV microgrid, validating its performance in seven quasi-stationary scenarios and providing practical sizing and prototyping criteria.

Control and bidirectionality. Stable operation in buck/boost with i_L continuity and reliable power flow management in both directions was verified.

Dynamic decoupling. The supercapacitor absorbed/delivered the fast component, reducing I_{bat} peaks and maintaining V_{bus} within the target ripple.

Sizing and feasibility. The ensemble L ≈ 80 µH, C_{bus} ≈ 1 mF, and 100 V MOSFETs at f_s = 20 kHz met the expected ripples and shows prototype feasibility (competitive specific cost for laboratory).

Bibliographic References

Ardi, H., Ahrabi, R.R., & Ravadanegh, S.N. (2014). Non-isolated bidirectional DC–DC converter: Analysis and implementation. *IET Power Electronics, 7*(12), 3033–3044. https://doi.org/10.1049/iet-pel.2013.0898

Eaton. (2023). *XLR-48 Ultracapacitor Module: Datasheet*. Eaton Corporation. https://www.eaton.com/us/en-us/catalog/energy-storage/xlr-48-ultracapacitor-module.html

Erickson, R.W., & Maksimović, D. (2020). *Fundamentals of power electronics*. Springer. https://doi.org/10.1007/978-3-030-43881-4

Faisal, M., Hannan, M.A., Ker, P.J., Hussain, A., Mansor, M.B., & Blaabjerg, F. (2018). Review of energy storage system technologies in microgrid applications: Issues and challenges. *IEEE Access, 6*, 35143–35164. https://doi.org/10.1109/ACCESS.2018.2841407

Infineon Technologies. (2017). *AN-978: HV floating MOS-gate driver ICs* (Application note). Infineon Technologies AG. https://www.infineon.com/dgdl/an-978.pdf

Jing, W., Lai, C., Wong, W.S. & Wong, M.L. (2017). Battery-supercapacitor hybrid energy storage system in standalone DC microgrids: a review. *IET Renewable Power Generation, 11*(4), 461–469. https://doi.org/10.1049/iet-rpg.2016.0500

Lai, C.M., Lin, Y.C., & Lee, D. (2015). Study and implementation of a two-phase interleaved bidirectional DC/DC converter for vehicle and DC-microgrid systems. *Energies, 8*(9), 9969–9991. https://doi.org/10.3390/en8099969

Lin, C.C., Yang, L.S., & Wu, G.W. (2013). Study of a non-isolated bidirectional DC–DC converter. *IET Power Electronics, 6*(1), 30–37. https://doi.org/10.1049/iet-pel.2012.0338

Liu, K.B., Yang, C.H., & Chang, E.C. (2016). Analysis and controller design of a universal bidirectional DC–DC converter. *Energies, 9*(7), 501. https://doi.org/10.3390/en9070501

Mohan, N., Undeland, T.M., & Robbins, W.P. (2003). *Power electronics: Converters, applications, and design*. Wiley.

Pérez-Aballe, O., Ruiz-Chavarría, G., Vázquez-Seis Dedos, L., & Columbié-Navarro, Ángel O. (2025). Diseño de convertidor DC/DC bidireccional dual para gestión de almacenamiento híbrido de energía en microrredes. *Minería y Geología, 41*(1), 83–101. https://revista.ismm.edu.cu/index.php/revistamg/article/view/2701

Pérez Aballe, O.R., Nicolas-Martin, C., González-García, J., Flores-Martín, P., & Santos-Martin, D.(2025). Sistema de Gestión de Energía en Microrred Eléctrica, con Almacenamiento Híbrido y Enfoque Multiobjetivo. *Revista Politécnica, 56*(1), 47–58. https://doi.org/10.33333/rp.vol56n1.04

Powersim. (2022). *PSIM 2022 R2 user manual*. Powersim Inc. https://powersimtech.com/resources/documentation/psim-user-manual/

Ramos, E., Del-Valle, Y., Santos-Canepa, R., & Loncoche-Cobarrubias, F. (2022). Hybrid energy storage systems: A review of filter-based methods for energy management. *Electronics, 11*(22), 3661. https://doi.org/10.3390/electronics11223661

Sutikno, T., Memon, A.A., Yusoff, A.M., & Jidin, A. (2023). Application of non-isolated bidirectional DC–DC converters. A review. *Clean Energy, 7*(2), 293–314. https://doi.org/10.1093/ce/zkad011

Tremblay, O., Dessaint, L A., & Dekkiche, A I. (2007). September). A generic battery model for the dynamic simulation of hybrid electric vehicles. In *2007 IEEE vehicle power and propulsion conference* (pp. 284-289). Ieee. https://ieeexplore.ieee.org/abstract/document/4544139/

Tremblay, O., & Dessaint, L.A. (2009). Experimental validation of a battery dynamic model for EV applications. *World Electric Vehicle Journal, 3*(2), 289–298. https://doi.org/10.3390/wevj3020289

Tshiani, C.T., & Umenne, P. (2022). The characterization of the electric double-layer capacitor (EDLC) using a Python/MATLAB/Simulink hybrid model. *Energies, 15*(14), 5193. https://doi.org/10.3390/en15145193

Tuluhong, A., Furqan, M., Ni, K., Liu, Z., Yu, Y., & Xie, X. (2025). Recent developments in bidirectional DC-DC converters: A comprehensive review. *Electronics, 14*(18), 3816. https://doi.org/10.3390/electronics14183816

Wang, J., Lin, Y., He, C., Zhang, T., & Li, H. (2022). Review of bidirectional DC–DC converter topologies for hybrid energy storage system of new energy vehicles. *Green Energy & Intelligent Transportation, 1*, 100010. https://doi.org/10.1016/j.geits.2022.100010

Winston Battery. (2024). *LiFePO4 LFP40AHA cell: Datasheet*. Winston Battery Ltd. https://en.winston-battery.com/index.php/product/proshow-120.html

Zhang, C., Li, K., Deng, J., & Song, S. (2017). A comparative study of RC equivalent circuit models for Li-ion batteries. *Applied Sciences, 7*(10), 990. https://doi.org/10.3390/app7100990

Zubieta, L., & Bonert, R. (2000). Characterization of double-layer capacitors for power electronics applications. *IEEE Transactions on Industry Applications, 36*(1), 199–205. https://doi.org/10.1109/28.821816

Conflict of Interest: The authors declare that there are no conflicts of interest.

Author's Contribution according to CRediT Taxonomy

Nancy Reynosa Casas: Investigation/Writing – original draft/Methodology
Yusbel Llorrente Cutiño: Formal analysis/Funding acquisition/Software
Christian E. Borges Alvarez: Software
Yilena Paumier Leyva: Investigation/Writing – review & editing
Osmany R. Pérez Aballe: Conceptualization/Methodology/Investigation/Writing – review & editing